

Laboratory simulation of heavy-ion cosmic-ray interaction with condensed CO

E. Seperuelo Duarte^{1,2,3}, A. Domaracka¹, P. Boduch¹, H. Rothard¹, E. Dartois⁴, and E. F. da Silveira²

¹ Centre de Recherche sur les Ions, les Matériaux et la Photonique (CEA/CNRS/ENSICAEN/Université de Caen-Basse Normandie), CIMAP - CIRIL - Ganel, Boulevard Henri Becquerel, BP 5133, 14070 Caen Cedex 05, France
e-mail: esduarte@gmail.com

² Physics Department, Pontifícia Universidade Católica, Rua Marquês de S. Vicente 225, 22453-900 Rio de Janeiro, Brazil

³ Grupo de Física e Astronomia - CEFET/Química de Nilópolis, R. Lúcio Tavares 1045, Centro, 26530-060, Nilópolis, Brazil

⁴ Institut d'Astrophysique Spatiale, Astrochimie Expérimentale, UMR-8617 Université Paris-Sud, bâtiment 121, 91405 Orsay, France

Received 16 July 2009 / Accepted 14 January 2010

ABSTRACT

Context. Within dense interstellar clouds, from their periphery to regions deep inside, ice mantles on dust grains are exposed to cosmic-ray irradiation. Various swift ions contribute from protons to iron in the keV to TeV energy range. Observations show that in some lines of sight condensed CO molecules are an important component of the ice.

Aims. We irradiate CO ices with Ni ions of relatively high energy (50 and 537 MeV) to simulate the effects produced by fast heavy cosmic-ray ions in interstellar grain mantles.

Methods. CO gas is condensed on a CsI substrate at 13 K and irradiated by 50 MeV $^{58}\text{Ni}^{13+}$ and 537 MeV $^{64}\text{Ni}^{24+}$ ions up to a final fluence of $\approx 1 \times 10^{13} \text{ cm}^{-2}$, at a flux of $1 \times 10^9 \text{ cm}^{-2} \text{ s}^{-1}$. The sputtering yields, the destruction rate of CO, and the rate of formation of new molecular species are measured in situ by Fourier transform infrared spectroscopy (FTIR).

Results. The measured CO destruction cross-sections and sputtering yields induced by Ni ions are, respectively, (i) for 50 MeV, $\sigma_d = 1.0 \times 10^{-13} \text{ cm}^2$ and $Y = 7 \times 10^4$ molecules/impact; (ii) for 537 MeV, $\sigma_d = 3.0 \times 10^{-14} \text{ cm}^2$ and $Y = 5.85 \times 10^4$ molecules/impact. Based on the present and previous results, the desorption rates induced by H, Ni, and Fe ions are estimated for a wide range of energies. The contribution of the heavy ions is found to dominate over that of protons in the interstellar medium.

Key words. astrochemistry – methods: laboratory – circumstellar matter – ISM: clouds – ISM: molecules

1. Introduction

Carbon monoxide is present in many astrophysical environments such as dense clouds and protoplanetary disks (e.g. Eiroa & Hodapp 1989; Tielens et al. 1991; Whittet & Duley 1991; Chiar et al. 1995; Elsila et al. 1997; Pontoppidan et al. 2003; Gibb et al. 2004; Dartois 2005; Bergin et al. 2006). CO has been observed in the gas phase as well as a condensed gas on dust grains. The abundance ratio of these two phases depends on the position of the grain in the cloud. At the cloud edge, because of the ambient interstellar radiation field, CO is predominantly in the gas phase (Shen et al. 2004). The external UV radiation cannot penetrate deeply into protoplanetary disks and dense clouds. Inside these objects, temperatures as low as 10 K may occur and CO molecules are expected to be present as ice on the grain mantles. According to estimations, the timescale to condense molecules ($\sim 10^9/n_{\text{H}}$ years; Watson 1975; Whittet 1992) is shorter than the estimated age of the cloud. However, the observation of molecules in the gas phase suggests the existence of a non-thermal desorption mechanism. As cosmic-rays are the only energetic particles capable of penetrating even the most shielded regions, different non-thermal desorption mechanisms involving these particles have been proposed in the literature: photodesorption by UV photons induced by cosmic rays (cosmic ray photodesorption; Prasad & Tarafdar 1983), collisional desorption by cosmic rays (sputtering), and the desorption by grain heating induced by cosmic rays (classical evaporation; Willacy & Millar 1998). Öberg et al. (2007) proposed that cosmic ray

photodesorption is comparable to the spot heating (desorption induced by a hot region at the ice surface created by cosmic ray impact) in the interior of the cloud.

A number of experimental studies involving chemical modifications of condensed carbon monoxide induced by different kinds of irradiation have been performed. Most of the experiments have included protons with energies ranging from 0.2 to 2 MeV (Baird 1972; Gerakines & Moore 2001; Trotter & Brooks 2004; Loeffler et al. 2005; Palumbo et al. 2008) and 10.2 eV Lyman- α photons (Gerakines et al. 1996; Gerakines & Moore 2001; Cottin et al. 2003; Loeffler et al. 2005). Jamieson et al. (2006) irradiated a CO sample with energetic electrons (5 keV). In all cases, infrared spectroscopy was used to probe modifications induced in the ice. Moreover, carbon monoxide ice has also been bombarded with noble gas ions (Harning et al. 1984; Chisey et al. 1986) and Cf fission fragments (Farenzena et al. 2006; Ponciano et al. 2006). In these cases, mass spectrometry was employed to analyze the reaction products.

There is a clear lack of information about the effects induced by the heavy-ion component of cosmic-rays in the electronic-energy-loss regime. Irradiation of CO₂ and mixed ices (NH₃:H₂O:CO and H₂O:NH₃) by Ni ions was studied by Seperuelo Duarte et al. (2009) and Pilling et al. (2010). The aim of our present work was to extend these measurements by simulating the astrophysical environment where ice grain mantles deep inside dense regions are subject to heavy-ion cosmic-ray irradiation. We irradiated condensed CO with 50 MeV $^{58}\text{Ni}^{13+}$ and 537 MeV $^{64}\text{Ni}^{24+}$ ion beams, and analyzed the products using

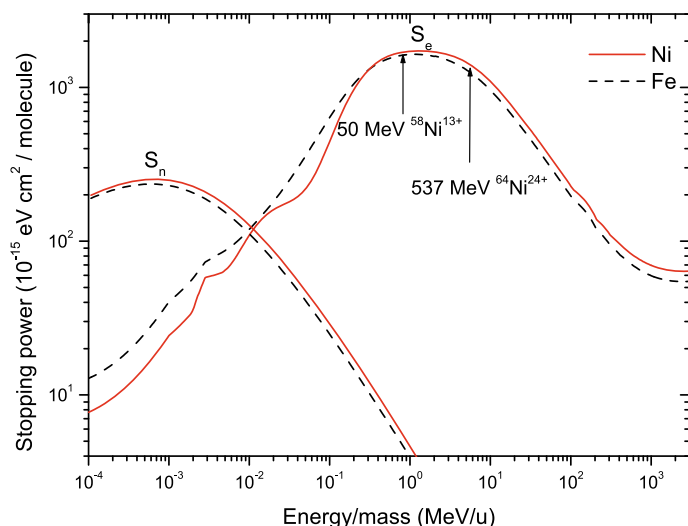


Fig. 1. Ni and Fe electronic (S_e) and nuclear (S_n) stopping power calculated by SRIM (Ziegler & Biersack 2006) for condensed CO film. Arrows show the conditions of the current experiment.

Fourier transform infrared spectroscopy (FTIR). The physics and chemistry induced by nickel ions are similar to those induced by other heavy ions (such as iron, one of the most abundant species) since their electronic stopping power (Fig. 1) and nuclear track structure within the ice are nearly identical.

2. Experimental

The experimental apparatus consists of three parts: the analysis chamber, the beam line, and the deposition system. The analysis chamber is inserted in a FTIR spectrometer. A CsI substrate is situated at the center of the chamber (Fig. 2) under a residual gas pressure of 2×10^{-8} mbar; it is in thermal contact with a cold finger cooled by a closed-cycle helium cryostat at a temperature of 13 K. The deposition system consists of: a pre-chamber, where the gas is prepared; a micro-valve to control the deposition flux; and a tube that connects the pre-chamber to the analysis chamber.

The ice film was produced by gas condensation onto the cold substrate. Infrared spectra in the $5000\text{--}600\text{ cm}^{-1}$ ($2\text{--}16.7\text{ }\mu\text{m}$) region are acquired using a Nicolet FTIR spectrometer (Magna 550) with a spectral resolution of 1 cm^{-1} . Since the main isotope transition is optically thick, the CO column density does not exhibit a linear relation with band area of the ν_1 fundamental vibration at 2138 cm^{-1} . Therefore, the ^{13}CO peak at 2092 cm^{-1} ($A = 1.3 \times 10^{-17}\text{ cm/molecule}$; Gerakines et al. 1995) was used to estimate the CO column density ($^{12}\text{CO} \approx 90 \times ^{13}\text{CO}$). For 50 MeV Ni ions, the initial column density was 1.6×10^{18} molecules/cm². The ice thickness of $0.94\text{ }\mu\text{m}$ was estimated using the initial column density, the CO molecular weight (28 g/mol), and the ice density of 0.81 g/cm^3 (Loeffler et al. 2005). In the case of 537 MeV Ni projectiles, two different ice thickness were irradiated: 5.8×10^{17} molecules/cm² ($0.34\text{ }\mu\text{m}$) and 1.04×10^{18} molecules/cm² ($0.60\text{ }\mu\text{m}$).

The experimental set-up was mounted on the IRRSUD beam line for 50 MeV ^{58}Ni and on the SME beam line for 537 MeV ^{64}Ni at the heavy-ion accelerator GANIL (Grand Accélérateur National d'Ions Lourds). The ices were irradiated by 50 MeV $^{58}\text{Ni}^{13+}$ and 537 MeV $^{64}\text{Ni}^{24}$ ions at a flux rate of $1 \times 10^9\text{ cm}^{-2}\text{ s}^{-1}$. The final fluences were $1.1 \times 10^{13}\text{ cm}^{-2}$ and $1.2 \times 10^{13}\text{ cm}^{-2}$, respectively. More details about the

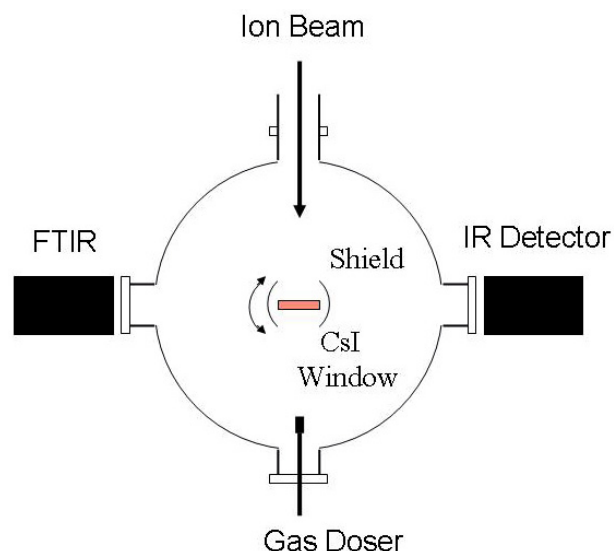


Fig. 2. A schematic representation of the experimental set-up. The ion beam impinges on the film ice deposited on a CsI substrate. A background spectrum is recorded at 13 K before gas deposition to correct the ice spectra.

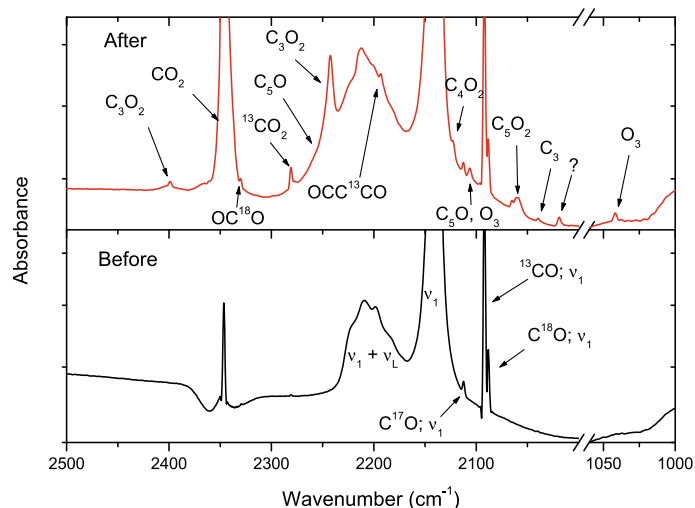


Fig. 3. Infrared spectrum of CO ice before and after 50 MeV $^{58}\text{Ni}^{11+}$ irradiation with a fluence of $1.0 \times 10^{12}\text{ cm}^{-2}$.

experimental set-up can be found in Seperuelo Duarte et al. (2009). At these energies, the energy loss is caused by the electronic stopping power (S_e) (see Fig. 1) since these ions interact with CO ice mainly via inelastic collisions with target electrons leading to ionization and excitation of the target electrons. For 50 MeV and 537 MeV Ni projectiles, the electronic stopping power values are $1690\text{ eV}/(10^{15}\text{ molecules/cm}^2)$ and $1180\text{ eV}/(10^{15}\text{ molecules/cm}^2)$, respectively.

3. Results

3.1. Line identifications

Table 1 shows the observed CO bands and a complete list of bands and associated molecules produced by heavy-ion irradiation. The same molecular species were observed at both 50 and 537 MeV. The CO_2 molecule is a common product of CO radiolysis, photolysis, as well as 5 keV electron irradiation

Table 1. Peak position and assignments for irradiated CO; *A* is the corresponding band strength.

Position (cm ⁻¹)	Molecule	Assignment	<i>A</i> (10 ⁻¹⁷ cm/molecule)	Reference
4694	?			
4252	CO	2ν ₁		Jamieson et al. (2006)
3707	CO ₂	ν ₁ + ν ₃		Gerakines et al. (1995)
3602	CO ₂	2ν ₂ + ν ₃		Gerakines et al. (1995)
3070	C ₃ O ₂	ν ₂ + ν ₃		Gerakines & Moore (2001)
2399	C ₃ O ₂	ν ₂ + ν ₄		Gerakines & Moore (2001)
2346	CO ₂	ν ₃	7.6	Yamada & Person (1964)
2330	OC ¹⁸ O	ν ₃		Jamieson et al. (2006)
2281	¹³ CO ₂	ν ₃		Gerakines et al. (1995)
2257	C ₅ O			Dibben et al. (2000)
2247	C ₃ O	ν ₁		Jamieson et al. (2006)
2242	C ₃ O ₂	ν ₃	13	Gerakines & Moore (2001)
2209	CO	ν ₁ + ν _L		Jamieson et al. (2006)
2193	C ₃ O ₂	ν ₁		Jamieson et al. (2006)
2139	CO	ν ₁	1.1	Jiang et al. (1975)
2123	C ₄ O ₂ or C ₇ O ₂	ν ₂		Jamieson et al. (2006)
2112	C ¹⁷ O	ν ₁		Palumbo et al. (2008)
2107	C ₅ O and O ₃	ν ₂ ; ν ₁ + ν ₃		Jamieson et al. (2006); Bennet & Kaiser (2005)
2092	¹³ CO	ν ₁		Gerakines et al. (1995)
2088	C ¹⁸ O	ν ₁		Jamieson et al. (2006)
2074	?			Freivogel et al. (1996)
2071	?			
2070	?			
2065	?			Szczepanski et al. (1996)
2060	C ₅ O ₂	ν ₃	7.4	Jamieson et al. (2006)
2039	C ₃	ν ₃	13	Jamieson et al. (2006)
2019	?			
1989	C ₂ O	ν ₁	2.4	Jamieson et al. (2006)
1950	C ₆			Trottier & Brooks
1915	C ₄ O	ν ₂		Jamieson et al. (2006)
1874	?			
1859	?			
1817	C ₅ O	ν ₃	6.2	Jamieson et al. (2006)
1303	?			
1041	O ₃		1.53	Bennet & Kaiser (2005)
879	?			
659	CO ₂	ν ₂		

(Loeffler et al. 2005; Jamieson et al. 2006; Trottier & Brooks 2004). In the present work, carbon dioxide is identified by means of its strong ν₃ and ν₂ fundamental lines at 2346 cm⁻¹ and 659 cm⁻¹, respectively. Three others lines related to CO₂ combination modes are also visible (see Table 1). The ν₃ vibration of the ¹³CO₂ is also observed at 2281 cm⁻¹ (Gerakines et al. 1995).

The peak at 1988 cm⁻¹ has been commonly attributed to the C₂O molecule (Palumbo et al. 2008; Jamieson et al. 2006; Trottier & Brooks 2004; Gerakines et al. 1996). Despite its simple formation reaction, this molecule has one of the lowest abundances of all detectable molecules in the present experiment. This means that C₂O may be an intermediate step in the formation of other molecules, such as C₃O and C₃O₂ (see in Sect. 4). In this experiment, C₃O is observed through a small shoulder at 2247 cm⁻¹ overlapped with an intense absorption line of C₃O₂ at 2242 cm⁻¹ (Dibben et al. 2000; Gerakines & Moore 2001).

A weak band at 2122 cm⁻¹ rises at the beginning of the irradiation ($F = 5 \times 10^{10}$ cm⁻²). Two different assignments were suggested in the literature: ν₂ vibration of the C₄O₂ molecule (Jamieson et al. 2006) and ν₆ vibration of the C₇O₂ molecule (Trottier & Brooks 2004). Since no other vibration mode produced by these molecules is present in the acquired spectra, it is not possible to confirm whether one or both molecular species contribute to this vibration.

Three different assignments were proposed for the band at 2107 cm⁻¹: the combination mode ν₁ + ν₃ of O₃ (Bennet & Kaiser 2005); the ν₂ vibration of the C₅O molecule (Jamieson et al. 2006); and the ν₁ - ν_L combination band of the C₃O₂ molecule (Gerakines & Moore 2001). The combination mode of C₃O₂ can be excluded since this molecule is highly diluted in the CO ice. In these circumstances, the lattice mode should not be active. The C₅O molecule may contribute to the 2107 cm⁻¹ band, because additional vibrations at 1817 cm⁻¹ and 2257 cm⁻¹ (Jamieson et al. 2006; Dibben et al. 2000) are observed in the current experiment. The O₃ molecule is clearly identified by detection of its ν₃ vibration at 1041 cm⁻¹ (Bennet & Kaiser 2005), showing that the abundance of oxygen atoms in the ice should be high. Therefore, the 2107 cm⁻¹ band is assigned to both molecules.

Palumbo et al. (2008) and Jamieson et al. (2006) observed a small band at ≈2065 cm⁻¹. In the current experiment, this band was also observed on top of a more intense band at ≈2060 cm⁻¹, which was attributed to the ν₅ vibration of the C₅O₂ molecule (Palumbo et al. 2008; Jamieson et al. 2006; Trottier & Brooks 2004).

The C₃ molecule was identified by the 2039 cm⁻¹ line (Weltner et al. 1964; Jacox & Milligan 1974; Cermak et al. 1998). In the current experiment, this peak rises early ($F = 1 \times 10^{10}$ cm⁻²) in the spectrum and disappears at high fluences

($F = 8.75 \times 10^{12} \text{ cm}^{-2}$) where the bands for complex molecules start to be come visible. This suggests that tricarbon molecules are precursors to the formation of long-chain carbon molecules. At a fluence of $5 \times 10^{10} \text{ cm}^{-2}$, a peak rises at 1950 cm^{-1} and disappears at $5 \times 10^{12} \text{ cm}^{-2}$. This line was attributed to a vibration of the C_6 molecule (Trottier & Brooks 2004). Finally, a peak at 2074 cm^{-1} appears in the spectrum corresponding to high fluences ($F = 5 \times 10^{12} \text{ cm}^{-2}$). There are many possible species that may absorb this wavenumber. Among them, C_{10} seems to be the most probable molecule to assign (Freivogel et al. 1997). This indicates that there has been an evolution of the long-chain carbon species formation from C_3 to C_{10} . However, further investigation is required to confirm this result. The peak at 1915 cm^{-1} rises at medium fluences ($F = 1 \times 10^{11} \text{ cm}^{-2}$) and disappears soon after ($F = 5 \times 10^{11} \text{ cm}^{-2}$). Among the many possibilities of assignment, C_4O is the most probable molecule responsible for this absorption (Palumbo et al. 2008; Jamieson et al. 2006; Trottier & Brooks 2004).

3.2. Quantitative analysis

Figure 4 shows the evolution of CO column density as a function of 50 MeV and 537 MeV nickel ions for all studied ices. The decreasing CO column density is related to the formation of other species (via CO dissociation) and to the sputtering induced by heavy ions. To analyze these effects, the data were fitted by Eq. (1) (Seperuelo Duarte et al. 2009) with two sets of parameters representing the sputtering and the dissociation, which are the processes given by:

$$N = N_0 \exp(-\sigma_d F) - Y/\sigma_d (1 - \exp(-\sigma_d F)), \quad (1)$$

where N_0 is the initial column density, σ_d is the destruction-cross section, and Y is the sputtering yield. Therefore, IR spectrometry does not directly measure the sputtering yield but this can be obtained by analyzing the evolution of CO column density as a function of fluence. The obtained values of destruction-cross sections and sputtering yields are presented in Table 2. The experiments performed with 537 MeV Ni ions for two different initial column densities confirmed that neither destruction cross section nor sputtering yield depend on thickness, because their estimated values are the same within the error-bars. This is not the case for very thin ices, where the influence of substrate and radiolysis products has to be taken into account. In future studies, the average values $\sigma_d = 3 \times 10^{-14} \text{ cm}^2$ and $Y = 5.85 \times 10^4 \text{ molecules/ion}$ will be used. These values are related to the lower energy transferred by the 537 MeV projectile. The obtained sputtering yield values, for the two Ni ion energies, are in close agreement with the predictions of Brown et al. (1984), who found a quadratic relation between sputtering yield and electronic stopping power ($Y \sim S_e^2$). We note that the sputtering yield infers the average number of CO molecules removed per impact. Brown et al. (1984) observed using quadrupole mass spectrometry that the CO molecules are the overwhelming dominant ejected species from ice. The emission of neutral clusters is also expected to produce a high yield, as discussed by Ponciano et al. (2008) for the condensed O_2 target. The sputtering of ion species from CO bombarded by 65 MeV heavy-ions was measured by Farenzena et al. (2006) using time-of-flight mass spectrometry, CO^+ being one of the most abundant secondary ion. Defining the radiochemical yield as $G = 100\sigma_d/S_e$, the values obtained for the 50 and 537 MeV Ni ions are $G = 5.9 \text{ molecules}/(100 \text{ eV})$ and $G = 2.5 \text{ molecules}/(100 \text{ eV})$, respectively.

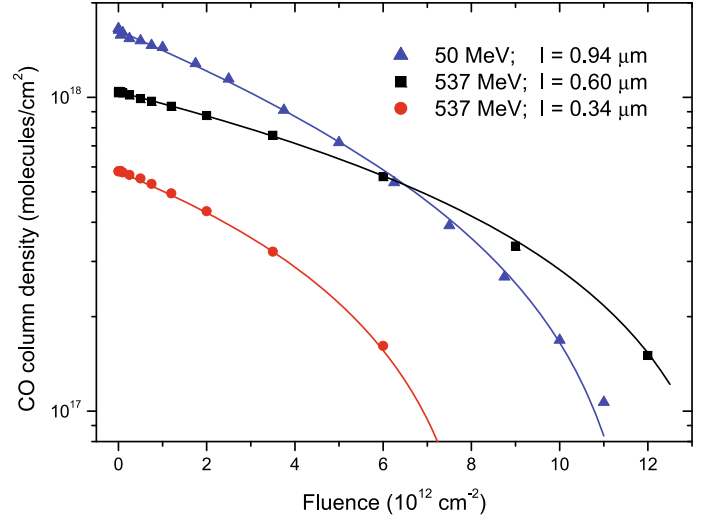


Fig. 4. Column density of CO molecules irradiated with 50 MeV and 537 MeV Ni ions as a function of fluence. The CO data are fitted by Eq. (1). The fitting results are presented in Table 2.

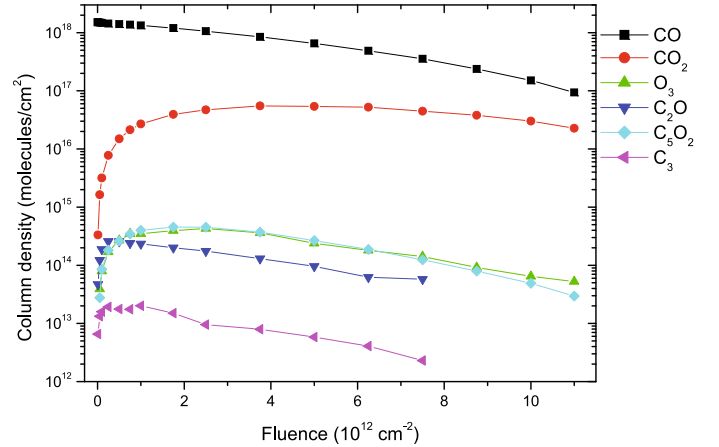


Fig. 5. Column density of CO and molecules produced as a function of fluence of 50 MeV Ni ions.

Figure 5 shows the evolution of the column density of species formed during irradiation by 50 MeV Ni ions as a function of fluence. CO_2 is the most abundant observable molecule formed in the ice. The abundance of some molecules (C_2O and C_3) have decreased to below the limit of detection at intermediate values of fluence.

The formation-cross sections of each molecular species were obtained from the slope of low fluence measurements, before the relative contribution of sputtering became important. Table 3 presents the formation cross sections and the corresponding radiochemical yields.

4. Discussion

4.1. Comparison with CO_2

The description of the reaction dynamics generated within a condensed solid irradiated by fast Ni ions is a difficult task. The energy deposited in matter is high enough to allow the existence of many different pathways to produce molecules. In the projectile track, multiple ionizations generate a flux of electrons that produce additional ionization, excitation, and/or dissociation. A complete description of these chemical reactions is beyond the scope of the present work. However, by comparing our present

Table 2. Destruction cross-sections and sputtering yields obtained for CO experiments.

Projectile energy (MeV)	CO column density (10^{17} molecules/cm ²)	Destruction cross-section (10^{-14} cm ²)	Sputtering yield (10^4 molecules/impact)
50	16.3	10.0 ± 0.1	7 ± 1
537	5.8	3.5 ± 1.0	5.8 ± 0.4
537	10.4	2.6 ± 0.3	5.9 ± 0.2

CO results (50 MeV) with those obtained for CO₂ irradiated by a 46 MeV Ni beam (Seperuelo Duarte et al. 2009), we can infer relevant information about the reactions occurring in the ice. These two samples have similar initial column densities and were irradiated by the same projectile with a very close energy. In the case of CO₂ ice, only four new species were observed: CO, CO₃, O₃, and C₃. In the present work, for CO ice, at least 10 new molecular species were identified, such as carbon-chain oxides and long carbon-chains. This difference is attributed to the higher reactivity of CO molecular fragments with respect to those of CO₂ just after the projectile interaction. The radiolysis products react preferentially with the most abundant species in the matrix, namely, CO molecules in the current experiment. Since CO₂ is less reactive, it acts like a shielding cage preventing the formation of large molecules.

Another clue about chemical reactions could be obtained by analyzing the common products observed in both experiments: C₃ and O₃. The formation cross-section of the O₃ molecule is one order of magnitude higher in the CO₂ experiment, probably because two CO₂ molecules react to form CO and O₂ (2CO₂ → 2CO + O₂). In the case of C₃ molecules, their low abundance in the CO₂ experiment prevents the measurement of their formation-cross section. This can be understood since the main dissociation pathways in the CO₂ experiment do not produce carbon atoms. In contrast, two CO dissociation pathways produce carbon atoms, which increases the abundance of C₃.

A comparison between CO and CO₂ ices bombarded by heavy ions and analyzed by mass spectrometry was discussed by Ponciano et al. (2006). For CO ice, they observed that a large quantity of unbound carbon is generated in the nuclear track (CO⁺ + CO → CO₂ + C⁺), which in turn produces carbon chains. For CO₂ ice, carbon chains are not observed but, instead, the CO₂ molecular dissociation liberates negative oxygen ions that in turn react with CO₂ to produce CO₃⁻ radicals. These findings are in perfect agreement with the present results.

4.2. Comparison with other experiments

Considering the CO radiolysis products from a qualitative point of view, the effects induced by nickel ions, protons (200 keV, Loeffler et al. 2005; Palumbo et al. 2008; 800 keV Gerakines & Moore 2001; 2 MeV, Trottier & Brooks 2004), photons (10.2 eV, Gerakines et al. 1996; Gerakines & Moore 2001; Cottin et al. 2003; Loeffler et al. 2005), and electrons (5 keV, Jamieson et al. 2006) are all similar. However, a striking difference occurs when observing ozone production. Loeffler et al. (2005) did not observe ozone in a CO ice irradiated by 200 keV protons. However, ozone was observed by Palumbo et al. (2008) using the same projectile with the same energy. In the current experiment, we agree with Palumbo et al. in observing the fundamental vibration of O₃ molecules (1041 cm⁻¹). This is experimental proof of an important production of oxygen atoms and molecules in the matrix [O₃/CO] ~ 10⁻³. However, it is surprising that the production of ozone can occur without carbon trioxide formation, which had been observed during the condensed CO₂ radiolysis

and photolysis. An explanation could be that CO₃ is readily destroyed when reacting with the CO matrix to produce CO₂ molecules.

Table 3 compares the cross-sections and radiochemical yields (G) calculated in the present experiment with published values. The negative G values for CO obtained in the current experiment correspond to the destruction cross-sections quoted in Sect. 3.2. Although the destruction G values estimated here are much higher than those for protons and photons, the formation G values of the produced molecules are similar. For CO₂ formation, the G values obtained in the current experiment are much higher than those for protons and photons. On the other hand, for the C₃O₂ molecule, the G value at 50 MeV is lower than that for 800 keV protons. It is interesting to note that the radiochemical yield of 537 MeV ions is an order of magnitude higher than that for 50 MeV ions. In the case of Ni ions, the formation G for CO₂ corresponds to 20% (50 MeV) and 60% (537 MeV) of the destruction G value for CO. For protons, this ratio is about 80% (which means that with Ni beam more different species are produced).

4.3. Astrophysical implications

CO molecules are observed in the gas phase below sublimation temperatures meaning that desorption processes are active. Among the possible processes, three general mechanisms are proposed: thermal desorption, photon-induced desorption, and cosmic-ray-induced desorption. In this latter case, spot heating (from a thermal spike around the ion track), but also whole-grain-heating (depending on the size of the grains) can contribute (Bringa & Johnson 2004). Thermal desorption and interstellar radiation field photodesorption are active essentially at the inner interfaces (close to a recently born star) and on the outer interfaces of the clouds (exposed to the interstellar radiation-field). In well protected extinct regions, where external UV photons do not penetrate, photodesorption can also take place because of cosmic-ray-induced secondary UV photons (e.g., Westley et al. 1995). Öberg et al. (2007) claimed that photodesorption dominates at the edge of dense clouds for small (0.1 μm) and large grains (of a few microns) and becomes comparable to the spot heating desorption inside the cloud ($A_V > 15$). Léger et al. (1985) estimated spot and impulsive (whole grain) heating desorption of about 70 molecules/cm² s by considering different heavy ions with $Z < 28$, energies between 20 and 1000 MeV/nucleon, and the abundances given by Young et al. (1981).

The results of the present work provide experimental insight into the understanding of desorption occurring in dense clouds via sputtering over the grain surface. The sputtering yield of Ni ions follows the proportionality to the square of the electronic stopping power ($Y \sim S_e^2$) found by Brown et al. (1984) (Fig. 6). This was used to estimate the desorption rate induced by heavy-ions from the grains in dense clouds.

By considering the $Y \sim S_e^2$ relation and the electronic stopping powers calculated by SRIM for Ni, Fe, and H ions crossing

Table 3. Cross-sections and radiochemical yields for molecules identified in present experiment.

Molecules	Projectile	σ (10^{-15} cm ²)	G (molecules/100 eV)	Reference
CO	50 MeV Ni ¹³⁺	100	-5.9	This work
	537 MeV Ni ²⁴⁺	30	-2.5	This work
	200 keV H ⁺	0.28	-0.79	Loeffler et al. (2005)
	10.2 eV photons	0.0003		Loeffler et al. (2005)
	>6 eV photons	<0.000001		Cottin et al. (2003)
	>6 eV photons	<0.00008		Gerakines et al. (1996)
CO ₂	50 MeV Ni ¹³⁺	20	1.2	This work
	537 MeV Ni ²⁴⁺	18	1.5	This work
	200 keV H ⁺	6	0.62	Loeffler et al. (2005)
	800 keV H ⁺		0.25	Gerakines & Moore (2001)
	10.2 eV photons	0.017	0.59	Loeffler et al. (2005)
	10.2 eV photons		0.9	Gerakines & Moore (2001)
	>6 eV photons	0.000013		Gerakines et al. (1996)
O ₃	50 MeV Ni ¹³⁺	0.3	0.018	This work
C ₃ O ₂	50 MeV Ni ¹³⁺	3	0.18	This work
	537 MeV Ni ²⁴⁺	25	2.2	This work
	800 keV H ⁺		0.24	Gerakines & Moore (2001)
	10.2 eV photons		0.014	Gerakines & Moore (2001)
C ₅ O ₂	50 MeV Ni ¹³⁺	0.45	0.027	This work
	537 MeV Ni ²⁴⁺	0.23	0.02	This work
C ₂ O	50 MeV Ni ¹³⁺	2	0.12	This work
C ₃	50 MeV Ni ¹³⁺	0.15	0.0089	This work

Notes. The presented value for CO molecules are destruction cross-sections, while for other molecules the formation cross-sections are given.

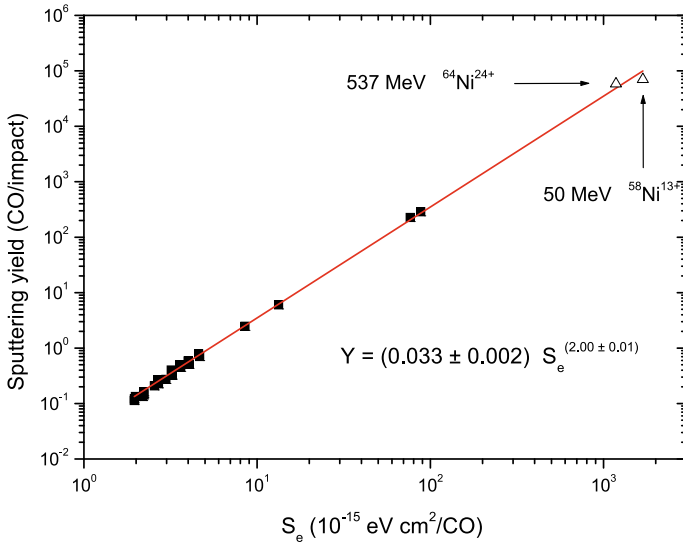


Fig. 6. Sputtering yield vs stopping power for CO ice. Full squares are the experimental points taken from Brown et al. (1984) and open triangles are present results for Ni ions.

a CO ice, the sputtering yield can be displayed as a function of the projectile energy (Fig. 7).

The cosmic ray abundance data were taken from Shen et al. (2004). The velocity distributions of heavy ions are very similar to those of protons (Simpson 1983) and the abundance ratios are Fe/H = 7.13×10^{-4} (Shen et al. 2004) and Ni/Fe = 5.5×10^{-2} (Karrer et al. 2007), respectively. This information allows us to estimate the desorption rates induced by H, Ni, and Fe ions as a function of projectile energy in the $5 \times 10^{-1} - 1 \times 10^4$ MeV/u range (Fig. 8). The total desorption rate (integrated over the aforementioned energy region) is indicated at the bottom of the figure.

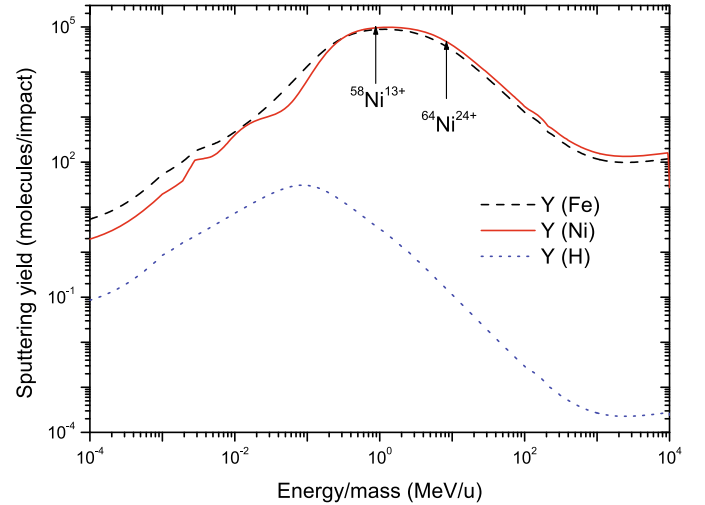


Fig. 7. Sputtering yield induced by H, Ni and Fe ions as a function of their energy/mass.

The maximum value of total desorption rate is obtained for iron ions.

Figure 9 shows the comparison between photodesorption, spot heating, and sputtering as a function of visual extinction values (A_V) of dense clouds. Photodesorption seems to be important at the edges of dense clouds where the stellar radiation-field is particularly active (Öberg et al. 2007). The S_e^2 dependence of the sputtering yield strongly favors the existence of heavy-ions in the cosmic-ray distribution and, for small grains, cause sputtering to dominate over the photodesorption in most of the cloud. We note that the desorption rate produced by iron ions alone is comparable to the rate of the desorption spot heating obtained by Léger et al. (1985), which also includes the

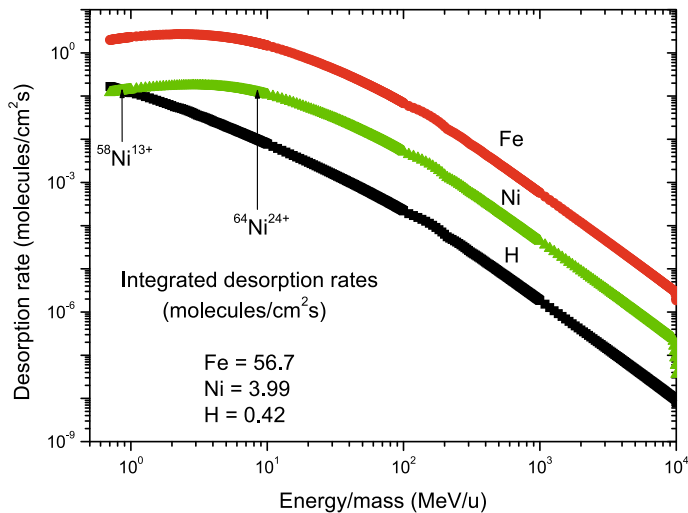


Fig. 8. Estimated desorption rates induced by H, Ni and Fe ions as a function of their energy/mass.

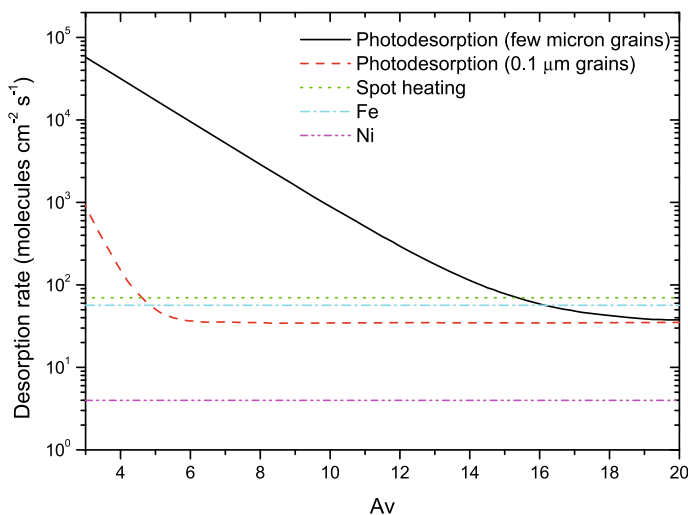


Fig. 9. Desorption rate of CO molecules as a function of visual extinctions. Photodesorption data for small and large grains are adopted from Öberg et al. (2007). The spot heating value was taken from Léger et al. (1985). The values presented for Ni and Fe are estimated from the results of the present work.

contribution of the other most abundant heavy-ion cosmic-ray species. This means that the true desorption rate produced by the contribution of heavy-ions in cosmic-rays may be even higher than the present estimations.

5. Conclusions

Condensed CO has been irradiated by 50 MeV $^{58}\text{Ni}^{13+}$ and 537 MeV $^{64}\text{Ni}^{24+}$ ions. The new species produced in the matrix are essentially the same as those found after proton, photon, and electron irradiations. The destruction and formation cross-sections, as well as the sputtering yields have been determined. The radiochemical yield for CO molecular destruction/dissociation by heavy-ion bombardment is much higher than those produced by weakly ionizing projectiles. The measured sputtering yields scale with the squared electronic stopping power values, extending to higher S_e the results of Brown et al. (1984). Desorption induced by heavy-ion sputtering is proposed to be one of the two dominant processes leading to the

presence of gas phase CO molecules in grains deep inside dense clouds and protoplanetary disks.

Acknowledgements. The authors acknowledge the agencies COFECUB (France) as well as CAPES, CNPq and FAPERJ (Brazil) for partial support. It is a pleasure to thank E. Balanzat, Th. Been, M. Ferry, I. Monnet and Y. Ngonon-Ravache for technical assistance.

References

- Baird, T. 1972, *Carbon*, 10, 723
 Bennett, C. J., & Kaiser, R. I. 2005, *ApJ*, 635, 1362
 Bergin, E. A., Maret, S., van der Tak, F. F. S., et al. 2006, *ApJ*, 645, 369
 Bringa, E. M., & Johnson R.E. 2004, *ApJ*, 603, 159
 Brown, W. L., Augustyniak, W. M., Marcantonio, K. J., et al. 1984, *Nucl. Instr. Meth. B*, 1, 307
 Cermak, I., Forderer, M., Cermakova, I., et al. 1998, *J. Chem. Phys.*, 108, 10129
 Chiar, J. E., Adamson, A. J., Kerr, T. H., & Whittet, D. C. B. 1995, *ApJ*, 455, 234
 Chrissey, D. B., Boring J. W., Phipps, J. A., et al. 1986, *Nucl. Instr. Meth. Phys. Res. B*, 13, 360
 Chrissey, D. B., Brown, W. L., & Boring J. W. 1990, *Surf. Sci.*, 225, 130
 Cottin, H., Moore, M. H., & Bénilan, Y. 2003, *ApJ*, 590, 874
 Dartois, E. 2005, *Space Sci. Rev.*, 119, 293
 Dibben, M., Szczepanski, J., Wehlburg, C., & Vala, M. 2000, *J. Phys. Chem. A*, 104, 3584
 Eiroa, C., & Hodapp, K.-W. 1989, *A&A*, 223, 271
 Elsila, J., Allamandola, L. J., & Sandford, S. A. 1997, *ApJ*, 479, 818
 Farenzena, L. S., Martinez, R., Iza, P., et al. 2006, *Int. J. Mass Spectrom.*, 251, 1
 Freivogel, P., Grutter, M., Forney, D., & Maier, J. P. 1997, *Chem. Phys.*, 216, 401
 Gerakines, P. A., & Moore, M. H. 2001, *Icarus*, 154, 372
 Gerakines, P. A., Schutte, W. A., Greenberg, J. M., & van Dishoeck, E. F. 1995, *A&A* 296, 810
 Gerakines, P. A., Schutte, W. A., & Ehrenfreund, P. 1996, *A&A*, 312, 289
 Gibb, E. L., Whittet, D. C. B., Boogert, A. C. A., & Tielens, A. G. G. M. 2004, *ApJS*, 151, 35
 Haring, R. A., Pedrys, R., Oostra, D. J., et al. 1984, *Nucl. Instr. Meth. Phys. Res. B*, 5, 483
 Jacox, M. E., & Milligan, D. E. 1974, *Chem. Phys.*, 4, 45
 Jamieson, C. S., Mebel, A. M., & Kaiser, R. I. 2006, *ApJS*, 163, 184
 Jiang, G. J., Person, W. B., & Brown, K. G. 1975, *J. Chem. Phys.*, 64, 1201
 Karrer, R., Bochsler, P., Giammanco, C., et al. 2007, *Space Sci. Rev.*, 130, 317
 Loeffler, M. J., Baratta, G. A., Palumbo, M. E., Strazzulla, G., & Baragiola, R. A. 2005, *A&A*, 435, 587
 Öberg, K. I., Fuchs, G. W., Awad, Z., et al. 2007, *ApJ*, 662, L23
 Palumbo, M. E., Leto, P., Siringo, C., & Trigilio C. 2008, *ApJ*, 685, 1033
 Pilling, S., Seperuelo Duarte, E., da Silveira, E. F., et al. 2010, *A&A*, 509, A87
 Ponciano, C. R., Martinez, R., Farenzena, L. S., et al. 2006, *J. Am. Mass Spectrom.*, 17, 1120
 Ponciano, C. R., Martinez, R., Farenzena, L. S., et al. 2008, *J. Mass Spectrom.*, 43, 1521
 Pontoppidan, K. M., Fraser, H. J., Dartois, E., et al. 2003, *A&A*, 408, 981
 Prasad, S. S., & Tarafdar, S. P. 1983, *ApJ*, 267, 603
 Schmidt, R., Schoppmann C., Brandl, D., et al. 1991, *Phys. Rev. B*, 44, 2
 Seperuelo Duarte, E., Boduch, P., Rothard, H., et al. 2009, *A&A*, 502, 599
 Shen, C. J., Greenberg, J. M., Schutte, W. A., & van Dishoeck, E. F. 2004, *A&A*, 415, 203
 Strazzulla, G., Leto, G., LaDelfa, S., Spinella, F., & Gomis, O. 2005, *Mem. S. A. It. Suppl.*, 6, 51
 Szczepanski, J., Ekern, S., Chapo, C., & Vala, M. 1996, *Chem. Phys.*, 211, 359
 Tielens, A. G. G. M., Tokunaga, A. T., Geballe, T. R., & Baas, F. 1991, *ApJ*, 381, 181
 Trotter, A., & Brooks, L. B. 2004, *ApJ*, 612, 1214
 Watson, W. P. 1975, *Atomic and Molecular Physics and the Interstellar Matter*, ed. R. Balian, P. Encrenaz, & J. Lequeux (Amsterdam: North-Holland)
 Weltner, W. Jr., Walsh, P. N., & Angell, C. L. 1964, *J. Chem. Phys.*, 40, 1299
 Westley, M. S., Baragiola, R. A., Johnson, R. E., & Baratta, G. A. 1995, *Plan. Space Sci.*, 43, 1311
 Whittet, D. C. B. 1992, *Dust in the Galactic Environment*, second edition (Institute of Physics Publishing)
 Whittet, D. C. B., & Duley, W. W. 1991, *A&AR*, 2, 167
 Willacy, K., & Millar, T. J. 1998, *MNRAS*, 298, 562
 Yamada, H., & Person, W. B. 1964, *J. Chem. Phys.*, 41, 2478
 Young, J. S., Freier, P. S., Waddington, C. J., & Brewster, N. R. 1981, *ApJ*, 246, 1014
 Ziegler, J. F., & Biersack, J. P. 2006, www.srim.org, version 2006.02